Egypt. J. Chem. **Vol. 65,** No. 10 pp. 195 - 202 (2022)

Egyptian Journal of Chemistry

http://ejchem.journals.ekb.eg/

Impacts of Decomposition Atmosphere on Surface Properties and Crystal Structure Characteristics of Praseodymia

Basma A. A. Balboul *[a], Alzahra A. Abd El-Moula[b] , Randa F. Abd El-baki[c]

[a] *Chemistry Department, college of Science, Jouf University, P.O. Box 2014, Sakaka, Aljouf, Saudi Arabia*

[b] *Physics Department, college of Science, Jouf University, P.O. Box 2014, Sakaka, Aljouf, Saudi Arabia*

[c] *Chemistry Department, faculty of Science, New Valley University, El-Kharja, Egypt*

Abstract

Praseodymia or praseodymium oxide $PrO_{1.833}$ was prepared from praseodymium nitrate hydrate in different atmospheres of gases oxygen, argon, and a mixture of oxygen and argon (1:1). The crystal structure and surface characteristics of praseodymium oxide ($PrO_{1.833}$ and PrO_2) obtained as the final decomposition product were characterized by different techniques, using surface adsorption–desorption of N_2 (SBET), thermogravimetric analysis (TGA), and X-ray diffraction (XRD), the acidic properties of praseodymium oxide $PrO_{1.83}$ were tested by FTIR spectroscopy of adsorbed CO as a probe molecule. The results indicate that the decomposition atmosphere affects the surface area, porosity, and crystal structure of the obtained oxides. Oxygen atmosphere promotes the formation of PrO_2, whereas Argon and Argon/oxygen atmosphere promote the formation of $PrO_{1.833}$ with larger surface area and improved mesoporosity. The non-stoichiometric oxide $PrO_{1.833}$ displays different types of surface hydroxyl groups and two different types of Lewis acid sites as indicated by CO adsorptions.

Keywords*: praseodymia; $PrO_{1.833}$; surface properties; crystal structure; nanocatalyst.*

Highlights

- Featured structure characteristics of the oxygen deficient oxide catalyst $PrO_{1.833}$
- Highlight the effect of processing parameters; heating temperature, atmosphere, as well as the effect of precursor on the stoichiometry of an interesting oxide.
- Exploring the type of porosity and surface acidity of Praseodymium oxide surface as an important parameter for improved catalytic performance.
- CO probing accounts for strong Lewis acid sites on oxide surface

1. Introduction

Praseodymia is an interesting rare earth oxide, exceptionally distinguished from other rare earths by its remarkable crystallographic and electronic flexibility that makes it applicable for microelectronic [1] as well as surface chemical applications, such as sensors [2] and catalysis [3]. Praseodymium oxide Pr_6O_{11} is thermally stable up to 1000°C [4] and is a part of the Homologous series with a large number of phases between Pr_2O_3 and PrO_2 with the homologous formula $Pr_{(n)}O_{(2n-2)}$ where n increases with oxidation. The stoichiometric Formula Pr_2O_3 and PrO_2 adopt the hexagonal and fluorite structures whereas non-stoichiometric ones, PrOx (x= 1.833, 1.810, 1.800, 1.78, 1.714 and 1.670), are oxygen deficient modifications of the fluorite structure [5].

Pr_6O_{11} (or $PrO_{1.833}$) usually produced via thermal decomposition of many salts such as acetate [6,7], oxalate [8, 9, 10], formate [11], nitrate [12], adepate, and sebacate, [13], and citrate [14]. The observed phases depend on the precursor used, atmosphere and temperature of decomposition [4- 6, 10, 15].

Earlier investigations of Hussein [6] have pointed out that Pr_6O_{11} is highly active towards isopropanol decomposition. However, propylene selectivity was found to be lower compared to that of Pr_2O_3, because of the lower acidity of Pr_6O_{11} [15]. Acidity and basicity are paired concepts, which are very often invoked to explain the catalytic properties of divided metal oxides [16]. Knozinger [17] defined the criteria for the selection of Probe molecules for surface acidity measurements. A classification of such probe molecules was given by Lavalley [16]. The catalytic activity of many oxides in various petrochemical and petroleum-refining processes, such as isomerization, alkylation, cracking, aromatization,

*Corresponding author e-mail: *babalboul@ju.edu.sa*

Receive Date: 08 January 2022, Revise Date: 04 February 2022, Accept Date: 20 February 2022

DOI: 10.21608/EJCHEM.2022.114561.5228

and many others [18], is due to their Lewis and Brønsted acidities [19]. Low-temperature carbon oxide adsorption is the most efficient tool for studying Lewis and Bronsted acid sites. Its efficiency is due to the small size of the CO molecule and to the simplicity of its spectral pattern (one site has one absorption band in the IR spectrum).

As reported by Hussein et al [12], the decomposition of Praseodymium nitrate hexahydrate $Pr(NO_3)_3.\ 6H_2O$ in the atmosphere of air proceeded through eleven thermal events forming several intermediates and the final oxide $PrO_{1.833}$ at 600 °C.

In comparison to earlier studies of the decomposition of praseodymium oxalate nonahydrate $Pr_2(C_2O_4)_3.10H_2O$ in oxygen and nitrogen atmosphere [6], the results indicate that the decomposition pathways and the composition of the final oxide are completely dependent upon the atmosphere of gases, (i) Pr_2O_3 was the final product in an oxygen atmosphere, and (ii) $PrO_{1.83}$ was the final product in atmosphere of nitrogen. In another study, the effect of the decomposition atmosphere Oxygen O_2, Nitrogen N_2 and hydrogen H_2, on the decomposition course of Praseodymium acetate monohydrate [4]. The results indicate that the nature of the gas atmosphere of Pr $(CH_3COOH)\cdot H_2O$ thermal decomposition influences the composition, pore size distribution and surface catalytic activity and selectivity of praseodymium oxide yielding at 600 °C.

The present investigation, is intended to study the composition, structure, texture and surface acidity of Pr-oxide obtained by thermal decomposition of $Pr(NO_3)_3.6H_2O$ in different atmosphere of gases namely, oxygen, argon, and a mixture of both. The oxide samples formed at 600°C for 1hr were subjected to XRD, surface area measurements by N_2 -sorption, Scanning electron microscopy, and Surface acidity by carbon monoxide adsorption using IR-spectroscopic technique.

2. Experimental

2.1. Materials

Praseodymium nitrate hexahydrate, $Pr(NO_3)_3.6H_2O$ (99.9%) was used as received from (Aldrich USA). The calcination products were obtained at 600°C for 1hr in a flow of oxygen, argon and a mixture of oxygen and argon in equimolar ratios. The calcination temperatures were chosen on basis of the thermal analysis results reported earlier [12]. These calcination products are indicated throughout the text as the salt designation and the temperature applied followed by the nature of the gas atmosphere. Thus P600/A, P600/O and P600/O/A indicate decomposition products (prasedymia) of Praseodymium nitrate at 600°C for 1hr in argon atmosphere, oxygen atmosphere and in equal volumes of both oxygen and argon, respectively.

2.2. Methods of Characterization of the nano-catalyst:

X-ray powder patterns were obtained with a JSX-60 PA JEOL diffractometer (JAPAN) using CuKα radiation (λ =1.5416Å) with a Ni-filter. Based on scans in the range $4° \leq 2\theta \leq 60°$, d-spacing and relative intensities (I/I°) were matched with ASTM standard diffraction patterns in the ASTM powder diffraction file [20]. The three samples were mounted separately on aluminum stubs, evacuated to 10-3 torr, and pre-coated (20 min total: 5 min for each of the four sides) in a sputter-coater with a thin, uniform, Au/Pd film to minimize charging in the electron beam. The applied sputter voltage was 1.2- 1.6 kV. A JOEL 35CF (JAPAN) SEM operating at 20 keV was used to obtain electron images.

Nitrogen sorption isotherms were determined volumetrically at –196°C on a Micro metrics ASAP 2010 instrument at 77.3 K. The BET method was used to evaluate surface area based on data with relative pressures between 0.05 and 0.3, and with the assumption that, the nitrogen molecules occupy 0.162 nm^2 [21, 22] in the BET monolayer. The BJH method with the Halsey equation was used to evaluate pore size distribution [23]. All samples were degassed at 300ºC for 2 hours under evacuation at 10-5 torr. . The total pore volume was derived from the volume adsorbed at P/Po=0. The porosity was measured by adopting the Va-t method [21, 22]. For plotting the distribution curves, the input data were derived from the adsorption branch, since it has been emphasized that distribution curves calculated from the desorption branch will give a misleading picture of the pore structure, owing to blocking effects [21, 22]. The N_2-sorption isotherms were determined volumetrically at –196°C using a micro-apparatus based on the design of Lippens et al. [24]. The test samples were out-gassed at 200°C for 2h under evacuation at 10^{-5} torr.

IR- spectra of CO adsorption were taken by using a stainless steel cell described elsewhere [25]. The following standard procedure was adopted. The samples synthesized were pressed into ~ 10 mg.cm2 self-supporting pellets. To remove water and surface carbonates, the samples were heated at 400°C in oxygen for 30 minutes, evacuated at 10-6 Torr for 30 minutes, and then cooled under the same vacuum. At low-temperature adsorption experiments, CO gas was introduced into the sample-containing volume and cooled down to -196 °C without helium. The spectra were obtained with a Nicolet-510 FT/IR spectrometer, at 2 cm-1 spectral resolution by collecting 128 to 1024 scans depending on the spectral range studied. All the spectra in this work are background subtracted. The band positions were determined using OMNIC software. 12CO (Matheson. 99.995% purity) gas was used.

3. Results and Discussion

Pr6O11 samples prepared in this study were obtained as the final product during the decomposition

of Pr(NO3)3.6H2O at 600°C for 1 hour in an atmosphere of oxygen, argon and a mixture of both (1:1) ratio. In an earlier study [12], We reported that Pr6O11 ($PrO_{1.833}$) was the final product formed at 465°C during the decomposition of Pr(NO3)3.6H2O in an atmosphere of air (Fig. 1). The results brought about reveal that the decomposition course of the nitrate commences near 145 °C and terminates at ≥663 °C, encompassing eleven (I–XI) mass-loss thermal events. Results obtained showed the nitrate to dehydrate stepwise at 130- 250 °C, and then decompose stepwise to yield $PrO_{1.833}$ at ≥ 465 °C encompassing the formation of the unstable intermediates oxynitrates ($PrO_{0.25}.(NO_3)_{2.5}$ // $PrO.NO_3$ solid products (at 360– 430 ◦C) and NO, NO_2 and O_2 as primary gaseous products. Pr_6O_{11} ($PrO_{1.833}$) Obtained at 600 °C has a surface area of 46.3 m^2/gm..

3.1. Structural Characteristics:

The XRD diffraction was obtained for the calcination products at 600°C for 1 hr of Pr $(NO_3)_3.6H_2O$ in a different atmospheres of gases (O_2, inert gas of Ar, and mixed gases Ar and O_2) is shown in (Fig.2). The obtained data were consistent with the stoichiometric PrO_2 and the nonstoichiometric $PrO_{1.833}$ documented as PrO_δ formula where $\delta \leq 2$ [36, 59] as indicated by (JCPDS sheets 24-1006 and 06-0329, respectively). The results indicate that, both phase composition and crystallite sizes of PrO_2 and $PrO_{1.833}$ were influenced by both temperature and decomposition atmosphere. The obtained oxide $PrO_{1.833}$ is oxygen deficient modifications of the fluorite-type cubic structure, identical to that documented (ASTM No 6-329).

The three above-mentioned oxides show a diffraction pattern with eight reflections corresponding to (111), (200), (220), (311), (222), (400), (331), and (420) planes conforming the above-mentioned cubic fluorite-type structure. The XRD peak intensity of the (200) plane was relatively higher than the other reflections, indicating that the $PrO_{1.83}$ formation has a preferential growth along the (200) direction. Clearly, the diffractograms show differences in both intensity and width of the peaks, an aspect related to the crystallinity of the oxides. The diffraction peaks of the P600/A/O_2 and P600/A samples are more intense and slightly narrower than that of sample P600/O_2, indicating higher crystallinity. The applied gas atmosphere plays an important role in determining the final oxide formed during the course of formation. Therefore, the above results indicate that heating Praseodymium nitrate hydrate in oxygen atmosphere favors to transfer of the non-stoichiometric $PrO_{1.83}$ to PrO_2 leading to stoichiometric lattice ionic oxygen. On the other hand, calcination in an inert gas (Ar) favors the formation of lattice oxygen vacancies, forming activated gaseous oxygen molecules into O^-species. [26].

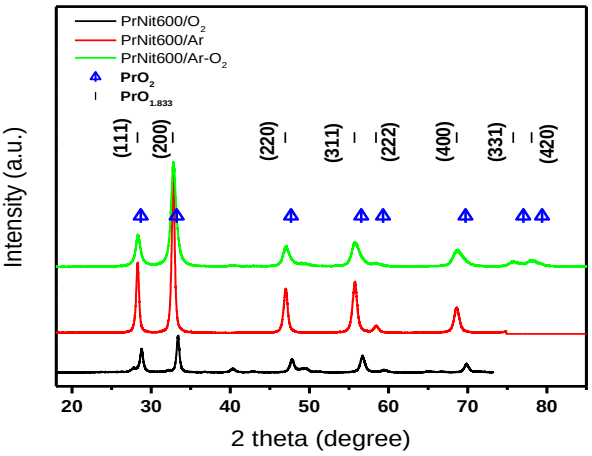

(Fig.1): X-ray powder diffractograms recorded for $Pr(NO_3)_3.6H_2O$ at 600°C for 1 hour in a different atmospheres of gases.

The crystallite size (D) of the three samples can be calculated from the full-width half-maximum (FWHM) values of the diffraction peaks. An average crystallite size (D) has been evaluated using Scherrer's equation [27].

$$D = \frac{K\lambda}{\beta \cos(\theta)} + 4\,\varepsilon \sin\,(\theta) \qquad (1)$$

Where λ the wavelength of the X-ray radiation, K is the Scherrer constant which is usually taken as K = 0.94, β is the full width at half maximum of a Gauss fit and θ Bragg's diffraction angle and ε is a strain. The crystallite size of the three samples was reported in table 1. The results in (fig. 1) revealed that, as the crystallinity of praseodymia enhanced, the crystallite size increased to reach 16.91 nm for P600/O_2, as the crystallite size increases the porosity and pore volume increase too (Table 1).

(Table1): The standard lattice parameter and surface of Pr $(NO_3)_3.6H_2O$ calcined at 600 °C for 1 hour in a different gas atmospheres

Lattice parameter	**P600/O/A**	**P600/O_2**	**P600/A**
Crystallite size (nm)	11.81	16.91	16.87
Strain	0.0038	0.00219	0.00211
Calculated Lattice constant (a)	a= 5.4569	a= 5.3838	a= 5.4660

The lattice parameter 'a' was calculated based on the interplanar spacing (d) using the following relationship

$$\frac{1}{d^2} = \frac{(h^2 + k^2 + l^2)}{a^2} \qquad \mathbf{(2)}$$

Where, h, k, and l are the Miller indices for the predominant orientation.

The standard lattice parameter for PrO_2 (a= 5.392Å) (JCPDS (24- 1006)) and the measured in table 1 for sample Pr600/O_2 (a = 5.3838 Å) confirmed the existence of stoichiometric phase PrO_2 in this sample, while the calculated lattice parameter for the other

calcinated samples confirmed the existence of non-stoichiometric phase $PrO_{1.833}$, with the standard (5.4695 Å). The crystal structure obtained by visualization and molecular visualization and functional program, diamond software, was presented in Fig. 3.

3.2. Surface Texture

The N_2 -adsorption-desorption isotherms were measured to investigate the specific surface area. The N_2- adsorption studies at -196°C on P600/A, P600/O, and P600/A/O were shown in (Fig. 3a). The isotherms of the three samples have nearly the same character, generally belong to type IV of the BET classification [21]. The hysteresis loops are nearly of type H3. According to the general characteristics, the pore structures are slit-shaped and/ or interplating pores. Texture data, the specific surface area (S_{BET}), BET- constant, and the total pore volume (Vp) were summarized in Table 1. The texture data in (Table 1) reveals the increase in Vp for P600/A, while the PSD curves (Fig.3b and 3c) exhibit a wider spectrum of mesoporosirty. P600/A may have a more porous character than that of the other two samples (P600/O and P600/A/O). Accordingly, one may suggest that the structure volume is associated with internal surface. The development of gaseous components during the decomposition course leads to the formation of accessible porous textures [21]. The development of fast transport channels (pores) throughout the bulk material is caused by the release of volatile components. In contrast, heat-induced mass transfer and sintering processes tend to eliminate pathways thus generated. Eventually, the absence and presence of accessible surface porosity is a question of the dominance of these two opposing effects. Finally, the type and amount of porosity may govern the extent to which densely packed crystal planes could grow larger [21]. This latter parameter was among those controlling the coordination unsaturation of surface.

Also, the PSD (Fig.3b) indicated that the P600/A has a higher amount of micro and mesoporosity in comparison to the other two samples, this is most probably the reason for the high area of P600/A. It seems that most of the pores originate sites and hence, the adsorption strength. Both adsorption characteristics (i.e., capacity and strength) were intimately related to adsorptive and catalytic performances of solids.

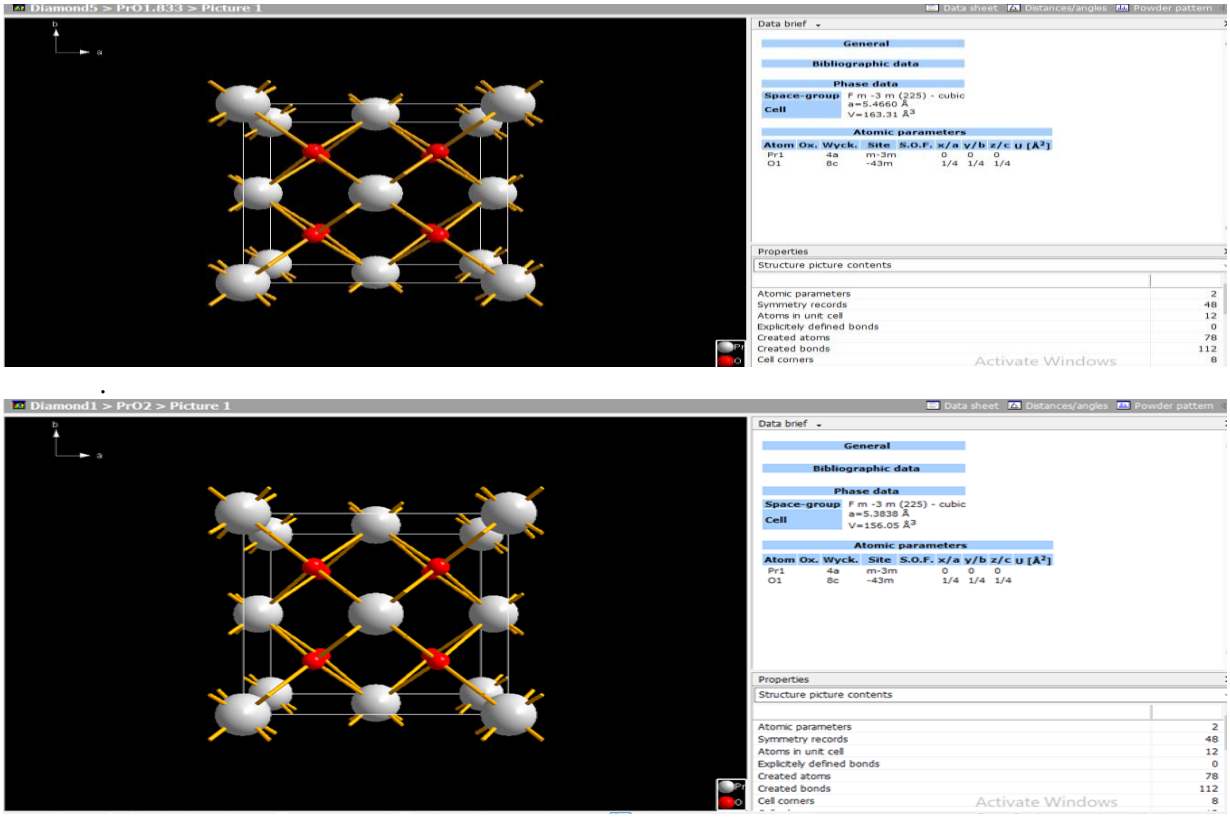

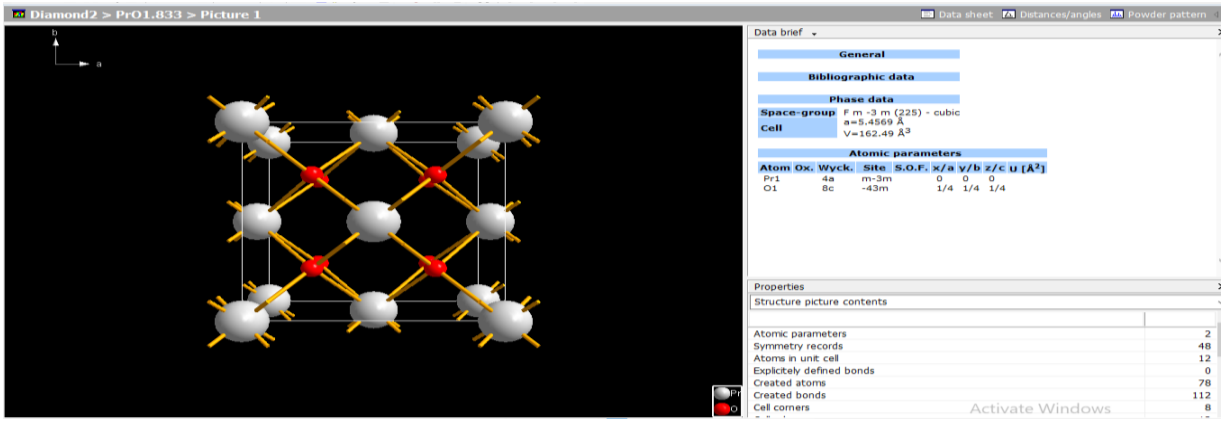

Fig. 2: Crystal structure for $Pr(NO_3)_3.6H_2O$ heat treated at 600°C for one hour in different atmosphere of gases.

The SBET for the P600/A sample (37.7 m2/ gm) was a little higher than that of both P600/O and P600A/O. The drop in the surface area for the later samples may be due to pore narrowing (sintering) (table 2).

Table 2: surface-textural characteristics of Pr(NO3)3.6H2O calcined at 600 °C for 1 hour in a different gas atmospheres.

surface-textural characteristics	P600/O/A	P600/O2	P600/A
BET Analysis			
C-value	132.2	88.4	62.7
SBET (m2/gm)	26.1	23.0	37.3
T-Plot Analysis			
Vp (pore volume) (cm3/gm)-	0.0182	0.0236	0.0324

Such pore narrowing effect can be taken as a consequence of the mass transfer involved in the sintering process.Also, the PSD (Fig.3b) indicated that the P600/A has a higher amount of micro and mesoporosity in comparison to the other two samples, this is most probably the reason for the high area of P600/A. It seems that most of the pores originate from either particle clusters and/or agglomerates [28] rather than pores from pores within particles. It was clear that the oxygen atmosphere enhances the sintering processes and also decreases the surface area forming PrO_2. It has been reported earlier that PrOx the oxygen-deficient phase has both high oxygen activity and excellent oxygen storage capacity which may lead to high catalytic activity. [29,30]. The above and the previous studies may conclude that not only does the atmosphere of gases applied during the decomposition course affect the composition of the final oxide product but also the nature and type of the precursor used is responsible for the chemical composition and structure of the final product.

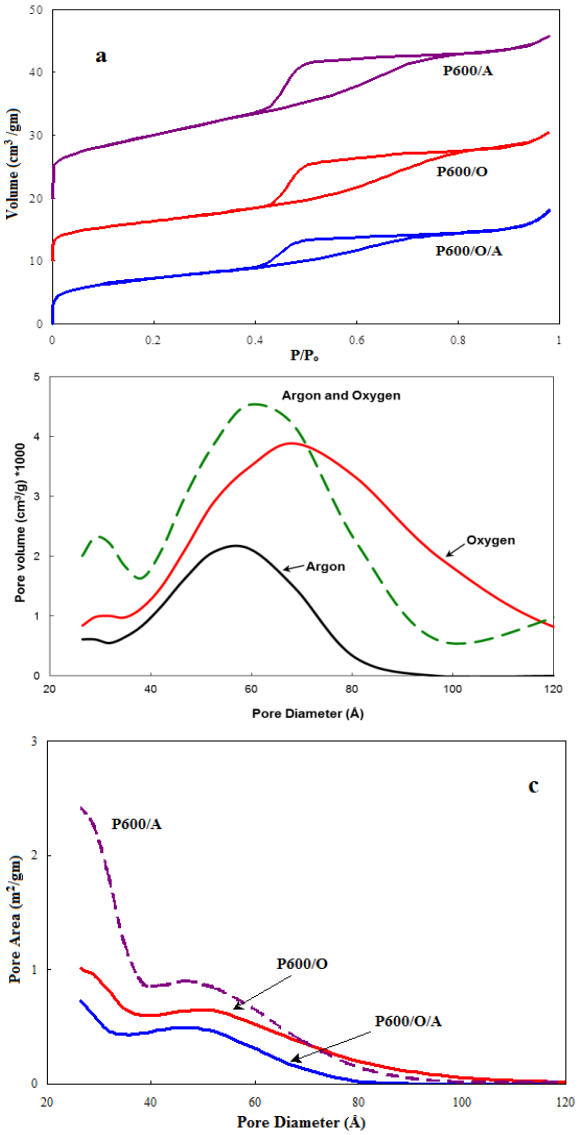

Figure 3: Nitrogen adsorption isotherm obtained for Praseodymium oxides in different atmosphere of gases at -195°C. (a), the corresponding Pore volume and pore area distribution curves (b) and (c).

3.2. Surface acidity by CO adsorption (IR spectroscopic studies)

The surface of the sample with the highest surface area P600/A was tested at 4000- 3300 cm^{-1} by carbon monoxide as a probe molecule to detect the presence and the nature of Lewis acidic sites as well as Brønsted sites to which it may H- bonded. Figure 4 (a and b), two spectral ranges were considered: that of the hydroxyl stretching mode [ν (OH), 3800-3400 cm^{-1}] section (a) of the figure and that of the C≡O stretching mode [ν(CO), 2250–2050 cm^{-1}; section (b) of the figure. Prior to CO adsorption, the initial FTIR spectrum of $PrO_{1.833}$ pretreated at 600 °C, exhibited a single weak ν (OH) band at 3445 cm^{-1}.

The spectrum of the higher surface area of the P600/A sample (Fig. 4a) over the range 3900 - 3300 cm^{-1} includes bands at 3775, 3765, 3650, 3585, and 3565 cm^{-1}. The overlapped bands (at 3775 and 3750 cm^{-1}) were due to isolated hydroxyl groups, while the next band at 3650 cm^{-1} was due to a bridging OH configuration of type II species. The fourth and fifth overlapped bands at 3585 and 3565 cm^{-1} were due to tridentate OH groups [31].

In the ν (CO) spectral region, bands at 2162 cm^{-1} and 2146 cm^{-1} in Fig. 4b and 5. At both low and high pressures of CO (0.9 and 10.2 Torr), two bands appear, for P600/A the first band at 2165 cm^{-1} and a second band at 2148 cm^{-1} developed with increasing the pressure with a little shift to lower wavenumber compared to the evacuated sample. After evacuation, the band at 2148 cm^{-1} nearly declined. However, the band at 2165 cm^{-1} remains a strong band.

The IR spectra of CO adsorbed on P600/O (dashed line) and P600/A/O measured at CO equilibrium pressure ≈0.4 and 10.2 Torr, were shown in (Fig. 5), respectively. FTIR measurements indicate that at low CO pressure at -196°C, CO adsorbs on Lewis acid sites of Praseodymium oxides. The slight shift to lower frequencies for adsorbed CO indicates a strong interaction of CO -adsorbed molecules with Lewis acid sites. The surface acidity property is of importance in the field of catalysis and renewable energy [33].

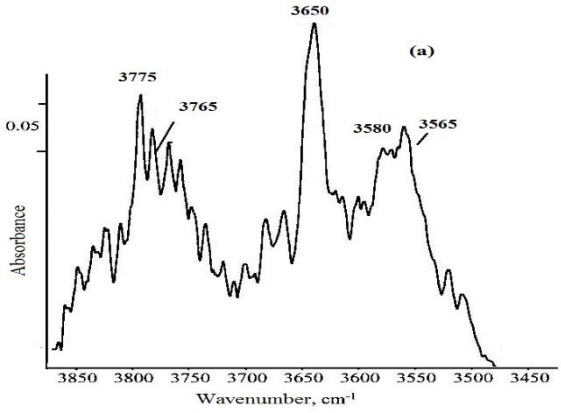

Fig. 4: IR spectra of CO adsorbed on P600/A, hydroxyl group region of the IR spectrum

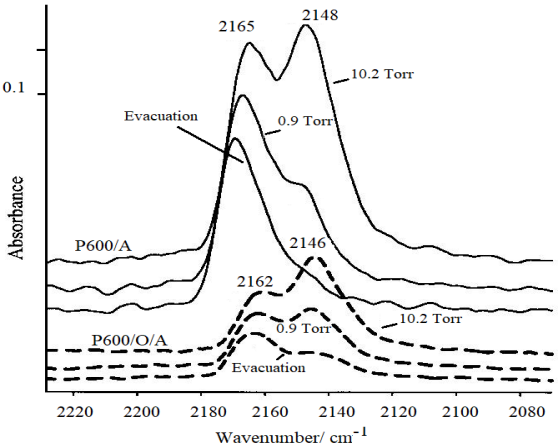

Fig. 5: IR spectra of CO adsorbed on P600/A ( ) and (———) P600/O/A (- - - -), CO equilibrium pressure ≈0.4 and 10.2 Torr.

4. Conclusion:

We have presented the crystal structure and surface characteristics of praseodymium oxide obtained as the final decomposition product in the different atmosphere of gases from praseodymium nitrate hydrate. The nature of the decomposition atmosphere and calcination temperature had an influence on the morphology and porous structure of the final oxides. Two samples obtained from $Pr(NO_3)_3.6H_2O$ in a different atmosphere of gases (Argon atmosphere and Argon/ Oxygen Atmosphere) have the same chemical composition $PrO_{1.833}$ and crystal structure which is oxygen deficient modifications of fluorite structure. The oxygen atmosphere enhances the formation of PrO_2 oxide. $PrO_{1.833}$ displays five different types of surface hydroxyl groups. Also shows two different types of Lewis acid sites as indicated by CO adsorptions. The results reveal the activity of praseodymia surface as a promising catalyst.

4. Conflicts of interest

There is no conflict of interest to declare.

5. References:

1. Schroeder T, Giussani A, Muessig HJ, Weidner G, Costina I, Wenger C., Lukosius M., Storck P., and Zaumseil P., Ge integration on Si via rare earth oxide buffers: From MBE to CVD, Microelectron. Eng. 2009; 86: 1615- 1620. doi.org/10.1016/j.mee.2009.03.108
2. Qian-Chun Zhang, Wu-Li Yan , Li Jiang , Yu-Guo Zheng , Jing-Xin Wang and Run-Kun Zhang, Synthesis of Nano-Praseodymium Oxide for Cataluminescence Sensing of Acetophenone in Exhaled Breath. *Molecules* 2019; 24: 4275. doi: 10.3390/molecules24234275.

3. Junjie Shi, Hailian Li, Weixuan Zhao, Pengfei Qi and Hongxin Wang, Praseodymium hydroxide/gold-supported precursor: a new strategy for preparing stable and active catalyst for the water-gas shift reaction. *Catal. Sci. Technol.* 2020;10: 7291-7301. doi.org/10.1039/D0CY01263G
4. Satoshi Sato, Ryoji Takahashi, Mika kobune and Hiroshi Gotoh. *Applied catalysis A*, 2009; 356: 57- 63. doi.org/10.1016/j.apcata.2008.12.019.
5. Gschneidner K A and Eyring L, The binary rare Earth Oxides in "Handbook on the chemistry and physics of Rare Earths" ed., Publ. North- Holand, 1979; 3: 337.
6. Hussein G A M, Formation of praseodymium oxide from the thermal decomposition of hydrated praseodymium acetate and oxalate, *J. Anal. Appl. Pyrolysis* 1994; 29:89-102. DOI: 10.1016/0165-2370(93)00782
7. Balboul B A A, Synthesis course and surface properties of praseodymium oxide obtained via thermal decomposition of praseodymium acetate: Impacts of the decomposition atmosphere, *Journal of Analytical and Applied Pyrolysis* 2011; 88: 192-198. 10.1016/j.jaap.2010.04.006
8. G A. M. Hussein, Characterization and activity of praseodymium oxide catalysts prepared in different gases from praseodymium oxalate hydrate. Microscopic, thermogravimetric and IR spectroscopic studies, J. chem. Soc. Faraday Trans. 91 (1995) 1385- 1390. doi.org/10.1039/FT9959101385
9. G. A. M. Hussein, Rare earth metal oxides: formation, characterization and catalytic activity Thermoanalytical and applied pyrolysis review, J. Anal. Appl. Pyrolysis, 37 (1996) 111. doi.org/10.1016/0165-2370(96)00941-2
10. Peng Lv, Liangjing Zhang, Sivasankar Koppala, Kaihua Chen, Yuan He, Shiwei Li, and Shaohua Yin, Decomposition Study of Praseodymium Oxalate as a Precursor for Praseodymium Oxide in the Microwave Field, ACS Omega 2020 5 (34), 21338-21344. DOI: 10.1021/acsomega.0c00505.
11. Y. Masuda, Thermal Decomposition of Scandium, Yttrium, and Rare Earth Metal Oxalates Thermochim Acta, 67 (1983) 271-285. doi.org/10.1021/ac60133a015
12. G. A. M. Hussein, B. A. A. Balboul, M. A. A-Warith and A.G.M. Othman, Thermal genesis course and characterization of praseodymium oxide from praseodymium nitrate hydrate Thermochimi Acta 369 (2001) 59. doi.org/10.1016/S0040-6031(00)00727-9
13. A. M. Wynne, J. E. Roberts, A thermogravimetric study of the adipates and sebacates of praseodymium and neodymium, Thermochim Acta 7(1973) 159-171. doi.org/10.1016/0040-6031(73)87018-2
14. M. Popa, M. Kakihana, Praseodymium oxide formation by thermal decomposition of a praseodymium complex, Solid State Ionics 141-142 (2001), 265 – 272, DOI: 10.1016/S0167-2738(01)00754-8.
15. Hussein, G M, Gates, B., Characterization of porous lanthanum oxide catalysts.Microscopic and spectroscopic studies, J. chem. Soc. Faraday Trans. 13 (1996) 3527 to 3780, doi.org/10.1039/FT9969202425
16. J. C. Lavalley, Infrared spectrometric studies of the surface basicity of metal oxides and zeolites using adsorbed probe molecules Catalysis Today 27 (1996) 377- 401. doi.org/10.1016/0920-5861(95)00161-1
17. H. Knözinger, Elementary Reaction Steps in R.W. Joyner and R. A. Van Santen (Editors), Heterogeneous Catalysis, Kluwer (1993) p.267.
18. Olah, G.A. and Molnar, A., Hydrocarbon Chemistry, New York: Wiley- Interscience, 1995.
19. Satterfield, Ch., Heterogeneous Catalysis in Practice, New York: McGraw- Hill, 1980.
20. J.V. Smith (ed.) X-ray Powder Data File, American Society for Testing and Materials, Philadelphia, USA, 1960.
21. S. J. Gregg and K.S.W. Sing, "Adsorption, Surface Area and Porosity" Academic press, London, 2nd edn., 1982.
22. F. Rouquerol, J. Rouquerol, K.S.W. Sing, "Adsorption by Powders and Porous Solids, Principles, Methodology and Applications, Academic Press, London, 1999.
23. M. A. Batavia, D. S. Bystrov, A. Yu. Kovalgin, A. A. Tsyganenko, J. Catal. 128 (1990) 396.
24. Lippens, B., Linsen B., and de-Boer, J., Studies on pore systems in catalysts I. The adsorption of nitrogen; apparatus and calculation, J. Catalysis, 3 (1964) 32-37. doi.org/10.1016/0021-9517(64)90089-2
25. Babaeva, M., Bystrov, D., Kovalgin, A., Tsyganenko, A., J. Catal., 1990, 128, 396
26. Slawomir Kuś, Marian Otremba, Artur Tórz, Marian Taniewski, The effect of gas atmosphere used in the calcination of MgO on its basicity and catalytic performance in oxidative coupling of methane, Applied Catalysis A: General, 230 (2002) 263–270. doi.org/10.1016/S0926-860X(02)00039-X
27. Cullity, B., eds., in: Elements of X-ray Diffraction, Addison-Wesley, 1978.
28. Sato, T. The thermal decomposition of zirconium oxyhydroxide. Journal of Thermal Analysis and Calorimetry 69, 255–265 (2002). https://doi.org/10.1023/A:1019962428910.
29. Cui, Y.; Lian, X.; Xu, L.; Chen, M.; Yang, B.; Wu, C.-E.; Li, W.; Huang, B.; Hu, X.

Designing and Fabricating Ordered Mesoporous Metal Oxides for CO_2 Catalytic Conversion: A Review and Prospect. Materials, 12 (2019) 276. doi: 10.3390/ma12020276

30. Sonström, P.; Birkenstock, J.; Borchert, Y.; Schilinsky, L.; Behrend, P.; Gries, K.; Müller, K.; Rosenauer, A.; Bäumer, M., Nanostructured Praseodymium Oxide: Correlation Between Phase Transitions and Catalytic Activity. ChemCatChem, 2010, 2, 694. doi.org/10.1021/jp0768524

31- Borchert, Y.; Sonström, P.; Wilhelm, M.; Borchert, H.; Bäumer, M., Nanostructured Praseodymium Oxide: Preparation, Structure, and Catalytic Properties, J. Phys. Chem. C, 2008, 112, 3054. doi.org/10.1021/jp0768524

32. Laachir, A., Fallah, J., Badri, A. Catherine, E., Lavalley, J., Reduction of CeO_2 by hydrogen. Magnetic susceptibility and Fourier-transform infrared, ultraviolet and X-ray photoelectron spectroscopy measurements, J. Chem. Soc. Faraday trans., 87(1991) 1601. doi.org/10.1039/FT9918701601.

33. Liu, H., Li, X., Dai, Q., Zhao, H., Chai G., , Guo, Y., Guo, Y., Wang, L., Zhan, W., Catalytic oxidation of chlorinated volatile organic compounds over Mn-Ti composite oxides catalysts: Elucidating the influence of surface acidity, Applied Catalysis B: Environmental, 282(2021) 119577. doi.org/10.1016/j.apcatb. 2020.119577